Supplemental Material

Hsiang-Hsuan Hung,[1] Lei Wang,[2] Zheng-Cheng Gu,[3,4] and Gregory A. Fiete[1]

[1]*Department of Physics, The University of Texas at Austin, Austin, TX, 78712, USA*
[2]*Theoretische Physik, ETH Zurich, 8093 Zurich, Switzerland*
[3]*Institute for Quantum Information, California Institute of Technology, Pasadena, CA 91125, USA*
[4]*Department of Physics, California Institute of Technology, Pasadena, CA 91125, USA*

(Dated: March 25, 2013)

PACS numbers: 71.10.Fd,71.70.Ej

Sign-free determinant projector QMC

The determinant QMC has been shown to be an excellent and unbiased approach to deal with strongly correlated system with Hubbard interactions.[1–8] In the projector algorithm, the ground state wave function $|\Psi_0\rangle$ can be obtained using standard projection procedures on a trivial wave function $|\Psi_T\rangle$, as long as one requires $\langle\Psi_T|\Psi_0\rangle \neq 0$. The expectation value of an observable A is obtained by

$$\langle A\rangle = \lim_{\Theta\to\infty} \frac{\langle\Psi_T|e^{-\frac{\Theta}{2}H}Ae^{-\frac{\Theta}{2}H}|\Psi_T\rangle}{\langle\Psi_T|e^{-\Theta H}|\Psi_T\rangle}. \tag{1}$$

The projection operator $e^{-\Theta H}$ can be discretized into many time slices $e^{-\Theta H} = [e^{-\Delta\tau H}]^M$ with $\Theta = \Delta\tau M$ where $\Delta\tau \ll 1$ and M is the number of time slices with a large integer number; $e^{-\Delta\tau H} = e^{-\Delta\tau(H_0+H_U)}$ is the imaginary time-evolution propagator during $\Delta\tau$. The noninteracting ground state of H_0 is a good candidate for the trial wave function $|\Psi_T\rangle$. With this trial wave function, we have confirmed that the determinant projector QMC is in a good agreement with our exact diagonalization results on a $L\times L = 3\times 3$ system. By the first order Suzuki-Trotter decomposition, one can decompose $e^{-\Delta\tau H}$ as

$$e^{-\Delta\tau H} \simeq e^{-\Delta\tau H_0}e^{-\Delta\tau H_U}, \tag{2}$$

where H_0 is the tight-binding Hamiltonian of the generalized Kane-Mele-Hubbard (KMH) model as shown in Eq. (1) of the main text. $H_U = \frac{U}{2}\sum_i (n_i-1)^2$ involves 4 fermionic operators and cannot be represented in terms of single-particle basis. However, by the discrete $SU(2)$-invariant Hubbard-Stratonovich transformation, [9] the interacting imaginary time-evolution operator $e^{-\Delta\tau H_U}$ (for $U>0$) can be decomposed as

$$e^{-\Delta\tau\frac{U}{2}(n_i-1)^2} = \frac{1}{4}\sum_{l=\pm1,\pm2}\gamma(l)e^{i\sqrt{\Delta\tau\frac{U}{2}}\eta(l)(n_i-1)} + O(\Delta\tau^4), \tag{3}$$

where $\gamma(\pm1) = 1+\sqrt{6}/3$, $\gamma(\pm2) = 1-\sqrt{6}/3$; $\eta(\pm1) = \pm\sqrt{2(3-\sqrt{6})}$ and $\eta(\pm2) = \pm\sqrt{2(3+\sqrt{6})}$ are 4-component auxiliary fields determined by Monte Carlo samplings. Ref. [10–12] provide pedagogical introductions about the QMC method. In this work, we employ $\Delta\tau t = 0.05$ in all the QMC simulations.

In the determinant algorithm with the Suzuki-Trotter decomposition Eq. (2) and the Hubbard-Stratonovich transformation Eq. (3), the denominator of Eq. (1) reads as [2, 10, 13, 14] (up to a constant factor)

$$\begin{aligned}\langle\Psi_T|e^{-\Theta H}|\Psi_T\rangle &= \langle\Psi_T|\prod_{\tau=1}^{M}e^{-\Delta\tau H_\tau}|\Psi_T\rangle = \langle\Psi_T|\prod_{\tau=1}^{M}e^{-\Delta\tau H_0}e^{-\Delta\tau H_{U,\tau}}|\Psi_T\rangle \\ &= \sum_{\{l_{i,\tau}\}}\Big\{\prod_{i,\tau}\gamma(l_{i,\tau})\prod_{\sigma}\mathrm{Tr}\Big(\prod_{\tau=1}^{M}e^{-\Delta\tau\sum_{i,j}c^\dagger_{i,\sigma}[\mathbf{H}^\sigma_{\mathbf{0}}]_{ij}c_{j,\sigma}}e^{i\sqrt{\Delta\tau\frac{U}{2}}\eta(l_{i,\tau})(n_{i,\sigma}-\frac{1}{2})}\Big)\Big\} \\ &= \sum_{\{l_{i,\tau}\}}\Big\{\prod_{i,\tau}\gamma(l_{i,\tau})p[\{\eta(l_i)\}]\Big\},\end{aligned} \tag{4}$$

where $\sum_{l_{i,\tau}}$ runs over possible auxiliary configurations $\eta(l_{i,\tau})$, where $i = 1-N$, $\tau = 1-M$; $\mathbf{H_0^\sigma}$ is the matrix kernel of H_0 with spin-σ. The probability weight p for a given auxiliary configuration $\{\eta(l_{i,\tau})\}$ is simply denoted as [15]

$$p(\{\eta\}) = \det\Big(O_\uparrow[\eta(l_{i,\tau})]\Big)\det\Big(O_\downarrow[\eta(l_{i,\tau})]\Big), \tag{5}$$

where $\det\Big(O_\sigma[\eta(l_{i,\tau})]\Big) = \mathrm{Tr}\Big(\prod_{\tau=1}^{M} e^{-\Delta\tau\sum_{i,j} c^\dagger_{i,\sigma}[\mathbf{H_0^\sigma}]_{ij}c_{j,\sigma}} e^{i\sqrt{\Delta\tau\frac{U}{2}}\eta(l_{i,\tau})(n_{i,\sigma}-\frac{1}{2})}\Big)$. When $p<0$, QMC simulations meet notorious minus-sign problems.

It has been proven, that at half filling, there exists a particle-hole symmetry in the Kane-Mele-Hubbard model (H_0 without t_{3N} terms), such that the probability is always positive-definitive.[13, 14] To show the positiveness of $p(\{\eta\})$ in the generalized KMH model, we employ the particle-hole transformation on the H_0 and H_U with $\downarrow$ but remain those with $\uparrow$ unchanged. The particle-hole transformation acts as

$$c_{i,\sigma} \to \xi_i d^\dagger_{i,\sigma}, \quad c^\dagger_{i,\sigma} \to \xi_i d_{i,\sigma},$$

where $\xi_i = -1$ ($\xi_i = 1$) if i belongs to A (B) sublattice. In the Kane-Mele-Hubbard model, upon such a transformation, the nearest-neighbor tight-binding term turns out to be

$$\begin{aligned} & -tc^\dagger_{i,\downarrow}c_{j,\downarrow} - tc^\dagger_{j,\downarrow}c_{i,\downarrow} \\ \to\ & -t\xi_i\xi_j d_{i,\downarrow}d^\dagger_{j,\downarrow} - t\xi_i\xi_j d_{j,\downarrow}d^\dagger_{i,\downarrow} = -t(d^\dagger_{j,\downarrow}d_{i,\downarrow} + d^\dagger_{i,\downarrow}d_{j,\downarrow}). \end{aligned}$$

Note that the t hopping connects A and B sublattices, so we have $(-1)\xi_i\xi_j = 1$. The correspondence spin-up term on the same $\langle i,j\rangle$ bond is $-t(c^\dagger_{i,\uparrow}c_{j,\uparrow} + c^\dagger_{j,\uparrow}c_{i,\uparrow})$. For the second-nearest-neighbor hopping term with spin-down, the particle-hole transformation acts it as

$$\begin{aligned} & i\lambda_{SO}c^\dagger_{i,\downarrow}c_{j,\downarrow} - i\lambda_{SO}c^\dagger_{j,\downarrow}c_{i,\downarrow} \\ \to\ & i\lambda_{SO}(-1)\xi_i\xi_j(d^\dagger_{j,\downarrow}d_{i,\downarrow} - d^\dagger_{i,\downarrow}d_{j,\downarrow}) = -i\lambda_{SO}(d^\dagger_{j,\downarrow}d_{i,\downarrow} - d^\dagger_{i,\downarrow}d_{j,\downarrow}). \end{aligned}$$

Here the $i\lambda_{SO}$ hopping connects the same sublattices, so we have $(-1)\xi_i\xi_j = -1$. The correspondence spin-up term on the same $\langle\langle i,j\rangle\rangle$ bond is $-i\lambda_{SO}c^\dagger_{i,\uparrow}c_{j,\uparrow} + i\lambda_{SO}c^\dagger_{j,\uparrow}c_{i,\uparrow}$. Thus, under the particle-hole symmetry, the tight-binding matrix kernel with the first and second nearest-neighbor hopping transforms as $\mathbf{H_0^\downarrow} \to \tilde{\mathbf{H}}_\mathbf{0}^\downarrow = \mathbf{H_0^{\uparrow\,*}}$, and thus the Kane-Mele-Hubbard model is particle-hole symmetric. For the third-nearest-neighbor hopping t_{3N}, the particle-hole transformation provides

$$\begin{aligned} & -t_{3N}c^\dagger_{i,\downarrow}c_{j,\downarrow} \\ \to\ & -t_{3N}\xi_i\xi_j d_{i,\downarrow}d^\dagger_{j,\downarrow} = -t_{3N}d^\dagger_{j,\downarrow}d_{i,\downarrow} \end{aligned}$$

unchanged since the t_{3N} hopping connects A and B sublattices. Therefore, the real-valued third-neighbor hopping t_{3N} in the generalized KMH model remains H_0 particle-hole symmetric at half-filling.

The Hubbard interaction H_U on $\downarrow$ transforms as

$$\begin{aligned} & i\sqrt{\Delta\tau\frac{U}{2}}\eta(l_{i,\tau})(n_{i,\downarrow} - \frac{1}{2}) \\ \to\ & i\sqrt{\Delta\tau\frac{U}{2}}\eta(l_{i,\tau})\Big\{(\xi_i)^2 d_{i,\downarrow}d^\dagger_{i,\downarrow} - \frac{1}{2}\Big\} \\ =\ & -i\sqrt{\Delta\tau\frac{U}{2}}\eta(l_{i,\tau})(d^\dagger_{i,\downarrow}d_{i,\downarrow} - \frac{1}{2}), \end{aligned}$$

which is the complex conjugate of H_U on $\uparrow$. Consequently, upon the particle-hole symmetry, one can have $\det(O_\downarrow) = \det(O_\uparrow)^*$ and the probability weight $p = \det(O_\uparrow)\det(O_\downarrow) = |\det(O_\uparrow)|^2$ being real positive. The QMC simulation in the half-filled generalized KMH model is sign-free and numerically exact.

single particle Green's functions and Z_2 invariant

Without sign problems, the QMC samplings provide highly accurate not only in equal-time Green's functions but also in time-displaced Green's functions[5, 16]

$$G_\sigma(\vec{r},\tau) = \langle\Psi_0|c_\sigma(\vec{r},\tau)c^\dagger_\sigma(0)|\Psi_0\rangle,$$

where $\tau > 0$. By performing double Fourier transformation we obtain the Green's functions in momentum space and with Matsubara frequency, i. e. $G_\sigma(\mathbf{k}, i\omega_n)$.

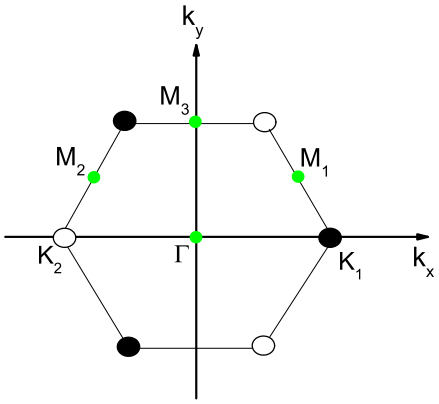

FIG. 1: (Color online) The Brillouin zone of the honeycomb lattice. The time-reversal invariant momentum (TRIM) points labeled by the green dots are $\Gamma = (0, 0)$, $M_{1,2} = (\pm\frac{\pi}{\sqrt{3}a}, \frac{\pi}{3a})$, and $M_3 = (0, \frac{2\pi}{3a})$. The open and solid circles denote graphene Dirac points $K_{1,2} = (\pm\frac{4\pi}{3\sqrt{3}a}, 0)$

.

It has been shown that the zero frequency Green's functions are able to evaluate the Z_2 invariant index in the interacting case.[17] The Z_2 invariant is determined by the parity of the eigenvectors of the inverse Green's functions on time-reversal invariant momentum (TRIM) points which are obtained from

$$[G(\mathbf{k}_i, 0)]^{-1}|\mu_i\rangle = \mu_i|\mu_i\rangle.$$

Note that since there still exists an inversion symmetry in the generalized KMH model, the inverse Green's functions and the parity operator have simultaneous eigenvectors, *i.e.* $P|\mu_i\rangle = \eta_{\mu_i}|\mu_i\rangle$. In the (generalized) KMH model, the parity operator exchanges A, B sublattices independent of spin index. Therefore, with the spinor convention $\Psi^\dagger = (c^\dagger_{A,\uparrow}\, c^\dagger_{B,\uparrow}\, c^\dagger_{A,\downarrow}\, c^\dagger_{B,\downarrow})$, the parity operator is defined as $P = I \otimes \sigma^x$.[18] In the QMC simulations, the particle-hole symmetry provides $G_\uparrow(\mathbf{k}_i, 0) = G_\downarrow(\mathbf{k}_i, 0)$, while $\mathbf{k}_i$ is at TRIM, i.e., $\mathbf{k} = -\mathbf{k} + \mathbf{G}$ for a reciprocal vectors $\mathbf{G}$. Therefore, we can directly diagonalize $G_\sigma(\mathbf{k}_i, 0) = [-H_\mathbf{k} - \Sigma(\mathbf{k}_i, 0)]^{-1}$ instead of inverse Green's functions for all $\mathbf{k}_i \in$ TRIM points

$$G_\sigma(\mathbf{k}_i, 0)|\tilde{\mu_i}\rangle = \tilde{\mu_i}|\tilde{\mu_i}\rangle,$$

and choose the eigenvectors associated with positive eigenvalues ($\tilde{\mu_i} > 0$, denoting occupied bands and are called right-zero [19]). In the honeycomb lattice, the TRIM points are Γ, $M_{1,2,3}$ as depicted in Fig. 1. Then we can employ the formalism proposed by Fu and Kane[18, 19] to evaluate the Z_2 invariant as

$$(-1)^\nu = \prod_{\mathbf{k}_i \in TRIM} \tilde{\eta}_{\mu_i}, \tag{6}$$

where $\tilde{\eta}_{\mu_i} = \langle\tilde{\mu_i}|P|\tilde{\mu_i}\rangle$. When $\nu = 0$ for a trivial insulator, whereas $\nu = 1$ for a Z_2 topological insulator. In the case of $U = 0$, $\tilde{\eta}_{\mu_i} = \pm 1$. In the cases of finite U, we find that $\langle\tilde{\eta}_{\mu_i}\rangle = \pm 1$ can be still obtained by sufficient QMC simulations. As t_{3N} approaches the topological critical point, $(-1)^\nu$ will be smeared out and is laid between ± 1. In this case, more QMC samplings are required for more accurate values.

Note that since $G_\uparrow(\mathbf{k}_i, 0) = G_\downarrow(\mathbf{k}_i, 0)$, and $G(\mathbf{k}_i, 0)$ $[= G_\uparrow(\mathbf{k}_i, 0) \oplus G_\downarrow(\mathbf{k}_i, 0)]$ and P $(= I \otimes \sigma^x)$ have the simultaneous eigenvector sets, one has a relation:

$$G_{\uparrow,\downarrow}(\mathbf{k}_i, 0) = \alpha_{\mathbf{k}_i}\sigma^x. \tag{7}$$

In the context we show that in addition to the Z_2 invariant, the proportional coefficient $\alpha_\mathbf{k}$ also plays another role to characterize the Z_2 topological insulator/trivial insulator phase transition and even is more sensitive than ν numerically. Upon the topological phase transition, the bulk gap will close at the TRIM points. Thus, the zero-frequency single-particle Green's functions are divergent on the poles. [20]

The relation Eq. (7) should be expected both in the noninteracting and interacting cases. However, as $U \neq 0$ Eq. (7) is not guaranteed in a single measurement in the QMC simulations. The proportionality relation between the zero-frequency Green's functions and the parity matrix σ^x can be recovered only upon enough samplings. To interpret this, we present the 6×6 benchmark results for the matrix elements of the zero-frequency Green's functions at $\mathbf{k}_i = M_1$ as a function of the number of measurements in Figs. 2. $g_{ij} = [G(\mathbf{M}_1, 0)]_{ij}$ and m denotes the number

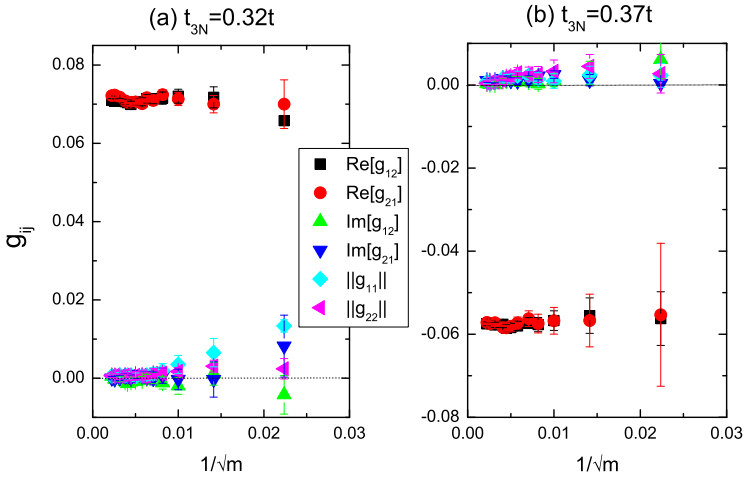

FIG. 2: (Color online) The matrix elements of the zero-frequency Green functions $G(\mathbf{M}_1, 0)$ vs the number of samplings m at (a) $t_{3N} = 0.32t$ and (b) $t_{3N} = 0.37t$. $\lambda_{SO} = 0.4t$ and $U = 4t$. Re$[g_{ij}]$ and Im$[g_{ij}]$ denote the real part and imaginary part of $[G(\mathbf{M}_1, 0)]_{ij}$, respectively; $||g_{ii}||$ denotes the diagonal component of $G(\mathbf{M}_1, 0)$ in magnitudes.

of measurements. $\lambda_{SO} = 0.4t$ and $U = 4t$ are used. In this case, the topological phase boundary is identified at $t_{3N} = 0.348t$. We choose the value of t_{3N} close to the critical point. Fig. 2 (a) shows $t_{3N} = 0.32t$ in the Z_2 topological insulator phase and (b) for $t_{3N} = 0.37t$ in the trivial insulator. From the panels, it is evident that the structure of the Green's function does not satisfy Eq. (7) without sufficient samplings. At small m, the real parts of g_{12} and g_{21} are not equal; furthermore, g_{12} and g_{21} have imaginary parts, and both of g_{11} and g_{22} are finite. However, one can see that, upon sampling sufficient times, Re$[g_{12}] \simeq$ Re$[g_{21}]$, and meanwhile Im$[g_{12}]$, Im$[g_{21}]$, $||g_{11(22)}||$ go to zero. Thus, in the $m \to \infty$ limit, Eq. (7) is recovered. Also note that, $\alpha_{\mathbf{M}_1} =$ Re$[g_{12}]$ in both cases indicates opposite sign as observed by the signature of the topological phase transition. Moreover, by such m scaling, we also confirm that, the value of the Z_2 invariant also monotonically approaches to ± 1. In our paper, we choose the value of m large enough to determine the σ^x structure and extract the coefficients, i.e., $\alpha_{\mathbf{k}_i}$ in Eq. (7).

Critical Hubbard interactions for antiferromagnetism

In the generalized KMH model, a strong Hubbard interaction can also derive the antiferromagnetic (AF) ordering, due to the bipartite lattice structure. Similarly to the KMH model (with $t_{3N} = 0$) [13, 21, 22], in the generalized KMH model, finite values of λ_{SO} also break the $SU(2)$ symmetry down to the $U(1)$ symmetry and the dominant magnetism behavior lies on x-y plane. The planar spin structure factor can be defined as[13, 22]

$$S_{AF} = \sum_{\vec{r},\vec{r}_j} (-1)^{\vec{r}_i + \vec{r}_j} \langle S_i^+ S_j^- + S_i^- S_j^+ \rangle.$$

$(-1)^{\vec{r}_i} = 1(-1)$ for $i \in A(B)$ sublattice. This is similar to determining the Néel type ordering using the antiferromagnetic spin structure factor at $\mathbf{k} = (\pi, \pi)$ in a square lattice.

To identify whether there exists the antiferromagnetism in the thermodynamic limit, we study the finite-size scaling behavior of S_{AF} at $L \to \infty$. Generally speaking, the spin-orbital coupling will suppress AF ordering, and larger λ_{SO}'s are associated with larger U_c's to induce the AF ordering. Note that, due to the presence of third nearest neighboring hopping t_{3N} which favors the Néel pattern in the second order perturbation, the threshold interaction U_c in the generalized KMH model is smaller than that in the KMH model.

The QMC results on S_{AF}/N vs $1/L$ are shown in Figs. 3. In (a), we can see that, for $\lambda_{SO} = 0.4t$, $U = 4t$ is not sufficiently large to induce the AF ordering. At $U = 5t$, S_{AF} is enhanced and the U value is close to the critical

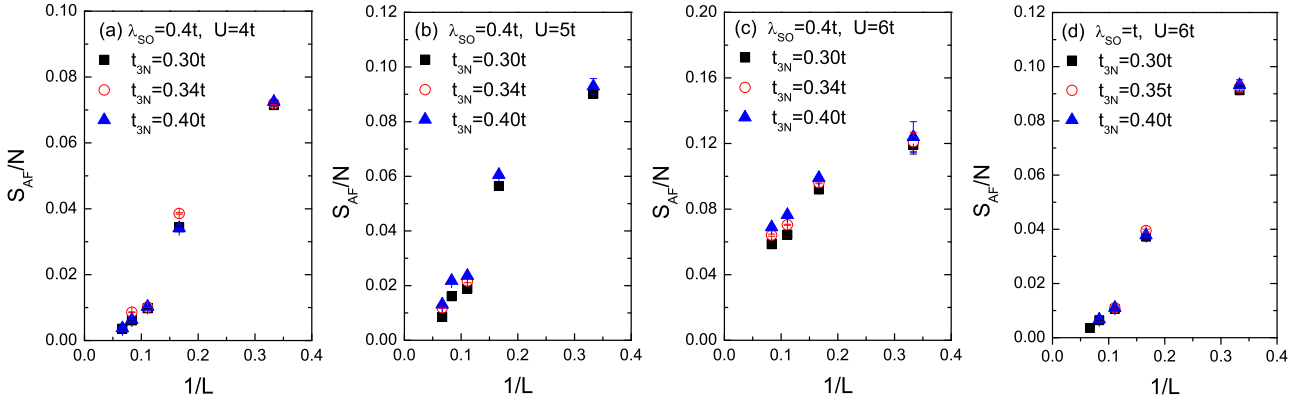

FIG. 3: (Color online) (a)-(c) The finite size scaling of the antiferromagnetic spin structure factor S_{AF}/N vs $1/L$ at $\lambda_{SO} = 0.4t$ and different $U = 4t, 5t, 6t$. (d) S_{AF}/N vs $1/L$ at $\lambda_{SO} = t$ and $U = 6t$. Here $N = 2 \times L^2$.

value to drive the AF ordering. In (c) under the interaction $U = 6t$, S_{AF} saturates to a finite value at $1/L \to 0$, suggesting that the AF ordering exists in the thermodynamic limit. Fig. 3 (d) depicts the case of $U = 6t$ but at $\lambda_{SO} = t$. Compared to (c), where an AF ordering is induced, the structure factor in (d) still goes to zero in the $L \to \infty$ limit. Thus, stronger spin-orbital couplings obviously suppress the existence of AF ordering and raise values of critical interactions U_c in the generalized KMH model.

Single-particle excitation

In this subsection, we present the approach to evaluate the single-particle excitation (charge gap) Δ_c in the QMC simulations. The charge gap is defined as the energy cost to add a particle into (or remove a particle from) the system composed of N_e fermions. Supposed that, $\hat{H}|\Psi_n^{N_e+1}\rangle = E_n^{N_e+1}|\Psi_n^{N_e+1}\rangle$ and $\hat{H}|\Psi_n^{N_e}\rangle = E_n^{N_e}|\Psi_n^{N_e}\rangle$, then the charge gap reads $\Delta_c \equiv E_0^{N_e+1} - E_0^{N_e}$. It can be obtained via calculating the on-site time-displaced Green's functions which are written as

$$\begin{aligned} G(\vec{r}=0,\tau) &= \frac{1}{N}\sum_{i,\sigma} G_\sigma(i,i;\tau) \\ &= \frac{1}{N}\sum_{i,\sigma}\langle\Psi_0^{N_e}|c_\sigma(i,\tau)c_\sigma^\dagger(i)|\Psi_0^{N_e}\rangle \\ &= \frac{1}{N}\sum_{i,\sigma}\langle\Psi_0^{N_e}|e^{\tau\hat{H}}c_\sigma(i)e^{-\tau\hat{H}}c_\sigma^\dagger(i)|\Psi_0^{N_e}\rangle. \\ &= \frac{1}{N}\sum_{n,i,\sigma} e^{-\tau(E_n^{N_e+1}-E_0^{N_e})}|\langle\Psi_0^{N_e}|c_\sigma(i)|\Psi_n^{N_e+1}\rangle|^2. \end{aligned}$$

Therefore, at large τ, we have $G(\vec{r}=0,\tau) \sim e^{-\tau\Delta_c}$ and then one can find the slope of $\ln G(\vec{r}=0,\tau)$ at large τ to determine the value of Δ_c. Refs. [5, 12, 16, 23] provide the detailed descriptions. The evaluation of the excitation by the on-site single-particle Green's function can determine the value of the single-particle excitation without concerning about specific momentum points, e.g. $\Delta_c(\mathbf{k})$. (Note that, in the noninteracting limit, the gap of the KMH model with $\lambda = 0$ closes at the Dirac points $K_{1,2}$, whereas the gap of the generalized KMH model with t_c closes at $M_{1,2,3}$.)

[1] G. Sugiyama and S. E. Koonin, Ann. Phys. **168**, 1 (1986).
[2] S. Sorella, S. Baroni, R. Car, and M. Parrinello, Europhys. Lett. **8**, 663 (1989).
[3] S. R. White, D. J. Scalapino, R. L. Sugar, E. Y. Loh, J. E. Gubernatis, and R. T. Scalettar, Phys. Rev. B **40**, 506 (1989).
[4] R. T. Scalettar, D. J. Scalapino, R. L. Sugar, and S. R. White, Phys. Rev. B **44**, 770 (1991).
[5] F. F. Assaad and M. Imada, J. Phys. Soc. Jpn. **65**, 189 (1996).

[6] F. F. Assaad, Phys. Rev. Lett. **83**, 796 (1999).
[7] Z. Y. Meng, T. C. Lang, S. Wessel, F. F. Assaad, and A. Muramatsu, Nature **464**, 847 (2010).
[8] Z. Cai, H.-H. Hung, L. Wang, Y. Li, and C. Wu, ArXiv e-prints:1207.6843 (2012).
[9] F. F. Assaad, ArXiv e-prints: cond-mat/9806307 (1998).
[10] F. F. Assaad, *Quantum Monte Carlo methods on lattices: The determinantal approach in Quantum Simulations of Complex Many-Body Systems: ¿From Theory to Algorithms, Lecture Notes* (NIC Series Vol. **10**, 2002).
[11] F. F. Assaad, AIP Conf. Proc. **678**, 117 (2003).
[12] H.-H. Hung, *Exotic quantum magnetism and superfluidity in optical lattices* (PhD thesis, University of California, San Diego, 2011).
[13] D. Zheng, G.-M. Zhang, and C. Wu, Phys. Rev. B **84**, 205121 (2011).
[14] M. Hohenadler, Z. Y. Meng, T. C. Lang, S. Wessel, A. Muramatsu, and F. F. Assaad, Phys. Rev. B **85**, 115132 (2012).
[15] J. E. Hirsch, Phys. Rev. B **31**, 4403 (1985).
[16] M. Feldbacher and F. F. Assaad, Phys. Rev. B **63**, 073105 (2001).
[17] Z. Wang and S.-C. Zhang, Phys. Rev. X **2**, 031008 (2012).
[18] L. Fu and C. L. Kane, Phys. Rev. B **76**, 045302 (2007).
[19] Z. Wang and S.-C. Zhang, Phys. Rev. X **2**, 031008 (2012).
[20] V. Gurarie, Phys. Rev. B **83**, 085426 (2011).
[21] S. Rachel and K. Le Hur, Phys. Rev. B **82**, 075106 (2010).
[22] M. Hohenadler, T. C. Lang, and F. F. Assaad, Phys. Rev. Lett. **106**, 100403 (2011).
[23] F. F. Assaad and M. Imada, Phys. Rev. Lett. **76**, 3176 (1996).